

Article

Synthesis, Structural, and Quantum Chemical Analysis of Neutral and Cationic Ruthenium(II) Complexes with Nicotinate-Polyethylene Glycol Ester Ligands

Dušan Dimić ^{1,†} , Thomas Eichhorn ^{2,†}, Dejan Milenković ³  and Goran N. Kaluđerović ^{2,*} 

¹ Faculty of Physical Chemistry, University of Belgrade, Studentski trg 12-16, 11000 Belgrade, Serbia; ddimic@ffh.bg.ac.rs

² Department of Engineering and Natural Sciences, University of Applied Sciences Merseburg, Eberhard-Leibnitz-Straße 2, 06217 Merseburg, Germany; thomas.eichhorn@hs-merseburg.de

³ Department of Science, Institute for Information Technologies, University of Kragujevac, Jovana Cvijića bb, 34000 Kragujevac, Serbia; dejanm@uni.kg.ac.rs

* Correspondence: goran.kaluderovic@hs-merseburg.de

† These authors contributed equally to this work.

Abstract: Ruthenium(II/III)-based compounds have gained significant interest due to the biocompatibility of ruthenium, its similarity to iron, and the possibility for structural diversification through the choice of ligands. In this contribution, two novel ligands, (2-(2-methoxyethoxy)ethyl nicotinate hydrochloride) and (2-[2-(2-methoxyethoxy)ethoxy]ethyl nicotinate hydrochloride) ($\text{pyCOO}(\text{CH}_2\text{CH}_2\text{O})_n\text{CH}_3$; **L2**, $n = 2$; **L3**, $n = 3$), were synthesized and characterized via ESI-HRMS, as well as IR and NMR spectroscopies. Their structures were optimized at the B3LYP/6-311++G(d,p) level of theory, and NMR chemical shifts were predicted, along with the most important intramolecular interactions. Additionally, two neutral complexes of the general formula $[\text{RuCl}_2(\eta^6\text{-}p\text{-cym})(\text{L-}\kappa\text{N})]$ (**L** = **L2**: **2**; **L3**: **3**) and two cationic complexes of the general formula $[\text{RuCl}(\eta^6\text{-}p\text{-cym})(\text{L-}\kappa\text{N})_2][\text{PF}_6]$ (**L** = **L1**: **4**; **L2**: **5**) were obtained and characterized. The optimization of the structures was performed at the B3LYP/6-31+G(d,p)(H,C,N,O,Cl)/LanL2DZ(Ru) level of theory. Structural features were described, and intramolecular stabilization interactions were outlined.

Keywords: ruthenium(II) complexes; nicotinic acid; polyethylene glycol esters; DFT; NMR



Citation: Dimić, D.; Eichhorn, T.; Milenković, D.; Kaluđerović, G.N. Synthesis, Structural, and Quantum Chemical Analysis of Neutral and Cationic Ruthenium(II) Complexes with Nicotinate-Polyethylene Glycol Ester Ligands. *Inorganics* **2023**, *11*, 460. <https://doi.org/10.3390/inorganics11120460>

Academic Editor: Jean Pierre Djukic

Received: 6 November 2023

Revised: 23 November 2023

Accepted: 25 November 2023

Published: 27 November 2023



Copyright: © 2023 by the authors. Licensee MDPI, Basel, Switzerland. This article is an open access article distributed under the terms and conditions of the Creative Commons Attribution (CC BY) license (<https://creativecommons.org/licenses/by/4.0/>).

1. Introduction

The discovery of cisplatin opened a new field in medicinal chemistry for using organometallic compounds as anticancer agents [1–4]. This compound was successfully applied to treat ovarian, cervical, bladder, testicular, and small-cell lung cancers [5]. Despite these benefits, cisplatin is often inflicted with severe side effects, such as peripheral neuropathy, emesis, fatigue, neurotoxicity, alopecia, and nephrotoxicity [6]. Therefore, it is of the utmost interest to further examine transition metal compounds using various experimental and theoretical methods, along with in vitro and in vivo studies. The presence of different ligands allows for the fine-tuning of important biological properties, such as lipophilicity, protein and DNA binding, and cytotoxicity. Special attention has been focused on the Pt group elements, which include palladium, ruthenium, iridium, rhodium, and osmium [7–9].

The ruthenium compounds are characterized by good cytotoxicity and antimetastatic activity, which makes them promising candidates against cancers with an acquired resistance towards commonly used drugs [10–15]. The discovery of the inhibitory effect of *fac*- $[\text{RuCl}_3(\text{NH}_3)_3]$ against *Escherichia coli* cell division marked the beginning of the extensive investigation of ruthenium compounds [16]. Several ruthenium compounds have shown a good selectivity between normal and tumor cell lines [17]. Numerous studies concerning

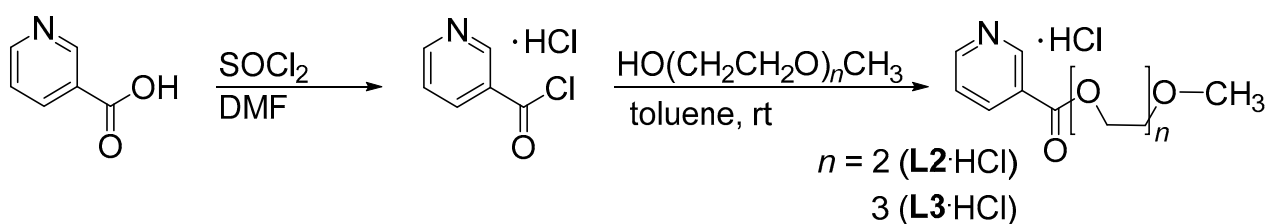
ruthenium compounds have been published, although two main classes can be distinguished: organometallic Ru(II)-arene and Ru(II)-polypyridine complexes [16]. The so-called “half sandwich” Ru(II)-arene compounds of the general formula $[(\eta^6\text{-arene})\text{Ru}(\text{YZ})(\text{X})]$, in which YZ is a bidentate or two monodentate ligands and X is a leaving group, represent a significant advancement in the preparation of Ru compounds [8,18]. These compounds allow for structural diversification through changing substituents on the arene group and choosing X, Y, and Z ligands. The latter substituents significantly improved the complexes' solubility, one of the major drawbacks in the first years of the ruthenium compounds investigation [19,20]. The increase in the number of halide groups is a focus of novel research due to the increased solubility of compounds [19,20]. Representatives of some ruthenium compounds in clinical trials are NAMI-A (imidazolium *trans*-[tetrachlorido(dimethyl sulfoxide)(1*H*-imidazole)ruthenate(III)]), KP1019 (indazolium *trans*-[tetrachloridobis(1*H*-imidazole)ruthenate(III)]), and the sodium salt analog of KP1019, namely NKP-1339 [21]. The cytotoxicity of Ru(II)-arene complexes was determined towards A2780 human ovarian cells and the effect of the size of arene ligands was proven with the activity of some complexes similar to cisplatin [22,23]. Complexes of the type $[(\eta^6\text{-arene})\text{Ru}(\text{en})\text{Cl}]^+$ were equally potent towards wild-type (A2780) and cisplatin-resistant (A2780cis) cells, which implied a different mechanism of action than that of cisplatin or carboplatin [24]. Ruthenium(II) arene complexes with *n*-octyl and pentamethylbenzyl ligands reduced tumor progression in a preclinical mouse model [25]. The antibladder cancer efficacy of complexes containing a 2,2'-bipyridine moiety was proven and described in the literature [26]. Ruthenium compounds with ethylenediamine, 1,3,5-triaza-7-phosphaadamantane, and isonicotinate ester moieties have shown promising in vitro and in vivo activity [22,24,27,28]. High activity against cancer prostate and colon cell lines was demonstrated for the binuclear Ru(II)-1-naphthylhydrazine complex [29].

In this contribution, two neutral complexes of the general formula $[\text{RuCl}_2(\eta^6\text{-}p\text{-cym})(\text{L}-\kappa\text{N})]$ (**L** = **L2**: **2**; **L3**: **3**) and two cationic complexes of the general formula $[\text{RuCl}(\eta^6\text{-}p\text{-cym})(\text{L}-\kappa\text{N})_2][\text{PF}_6]$ (**L** = **L1**: **4**; **L2**: **5**) were synthesized and characterized using elemental analysis, NMR, IR, and ESI-HRMS. Their ligand precursors, 2-(2-methoxyethoxy)ethyl nicotinate hydrochloride (**L2**·HCl) and 2-[2-(2-methoxyethoxy)ethoxy]ethyl nicotinate hydrochloride (**L3**·HCl), were also prepared and characterized. The structures of the complexes were optimized using the Density Functional Theory at B3LYP/6-31+G(d,p)(H,C,N,O,Cl)/LanL2DZ (Ru), and structural features were discussed. The Natural Bond Orbital Theory was applied to identify and quantify different stabilization interactions within a structure. The NMR spectra of **L2** were predicted using the Gauge Independent Atomic Orbital Approach to verify the applicability of the chosen level of theory.

2. Results and Discussion

2.1. Synthesis and Characterization of Ligands

Ligand **L1**·HCl was prepared as explained previously [29]. Analogously, the other two ligand precursors, **L2**·HCl and **L3**·HCl, were obtained in a similar reaction. Nicotinic acid was reacted with thionyl chloride, and the obtained acyl chloride hydrochloride, without purification, was used to prepare poly(ethylene glycol) esters **L2**·HCl and **L3**·HCl in high yields (95 and 92%, respectively; Scheme 1).



Scheme 1. Preparation of **L2**·HCl and **L3**·HCl.

The ESI-HRMS confirmed the molecular structure of the ligands. The solutions in methanol were prepared, and all samples showed simple isotopic patterns. Both ligands were found in a protonated form $[M + H]^+$: $[L2 + H]^+$ (226.10733 m/z) and $[L3 + H]^+$ (270.13355 m/z). The deviations between experimental and calculated values were lower than 0.3 ppm. As previously discussed for similar compounds [25], several characteristic bands were found in the IR spectra at 1730, 1280, 110, and 750 cm^{-1} . The band at 1730 cm^{-1} is assigned to the ester group. The position of this band was not dependent on the length of the alkyl chain. The other noticeable bands were the ones at 1280 and 1110 cm^{-1} assigned to carbon–oxygen single bonds in ether and ester groups [30]. The pyridine ring vibrations are located at 750 cm^{-1} . These vibrations can be overlapped with carbon–hydrogen vibrations in the fingerprint region. Wide bands can be observed in the area around 3000 cm^{-1} . Bands at 3020 cm^{-1} belong to the heteroaromatic vibrations of C–H bonds, while those at 2980 cm^{-1} can be attributed to C–H vibrations of alkyl groups. The NMR chemical shifts are commented on after the theoretical analysis and prediction of spectra.

2.2. Theoretical Analysis of the Structure of Ligands L1·HCl–L3·HCl

The structures of the ligands were optimized at the B3LYP/6-311++G(d,p) level of theory without any geometrical constraints. The absence of imaginary frequencies proved that the minima on the potential energy surface were obtained. The optimized structures of ligands L1·HCl–L3·HCl are presented in Figure 1.

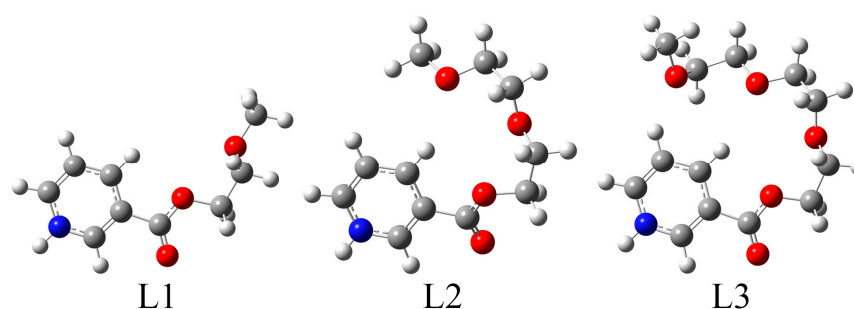


Figure 1. Optimized structures of ligands L1·HCl–L3·HCl: only HL^+ cations are shown, at B3LYP/6-311++G(d,p) level of theory (hydrogen—white, carbon—gray, nitrogen—blue, oxygen—red).

The structures of the ligands consist of a pyridine ring and an (poly)oxyethoxy chain. The part of a molecule that contains a pyridine ring and ester group is planar due to the extended delocalization, while the rest of the aliphatic chain is flexible. Figure 1 shows that certain deviations from the linearity of the aliphatic chain can be expected. To verify the applicability of the chosen level of theory and optimized structures, the NMR spectra of L2·HCl were calculated using the GIAO method. Table 1 lists the experimental and theoretical ^1H and ^{13}C NMR chemical shifts. The experimental and theoretical values were compared, exemplary herein for L2·HCl, by calculating the correlation coefficient (R) and mean absolute error (MAE). The values of ^{13}C NMR chemical shifts were systematically overestimated. The correction factor of 1.07 was obtained from the dependency of theoretical on experimental values for L2·HCl.

The theoretical ^1H NMR chemical shifts reproduce well the experimental ones, with a high correlation coefficient (0.997) and low MAE value (0.16 ppm). The lowest value of the hydrogen atom resonances in the ^1H NMR spectrum of L2·HCl is assigned to the terminal methoxy group (3.34 ppm in the experimental spectrum and 3.53 ppm in the theoretical spectrum). Two aliphatic chain methylene groups (4H) have equal chemical shifts of 3.79 (or 3.78 in the theoretical spectrum) ppm. The proximity of the ester group leads to the increased values of the chemical shifts of 3.97 and 4.66 ppm for $\text{OOCCH}_2\text{CH}_2$ and COOCH_2 , respectively. Hydrogen atoms of the pyridine ring have higher values of chemical shifts due to the aromaticity of a ring structure. The resonances of these atoms are located between 8.28 and 9.44 ppm in the experimental spectrum and between 8.44 and

10.00 ppm in the theoretical spectrum. It is important to observe that the chemical shifts of ligands **L1**·HCl and **L3**·HCl do not differ significantly from these mentioned values, as shown in the Methodology part and reference [29]. The chemical shifts of hydrogen atoms attached to the pyridine ring, carbonyl group, and ending methoxy group have almost identical chemical shifts within these three compounds.

Table 1. Experimental and theoretical (at B3LYP/6-311++G(d,p) level of theory) ^1H and ^{13}C NMR chemical shifts of **L2**·HCl.

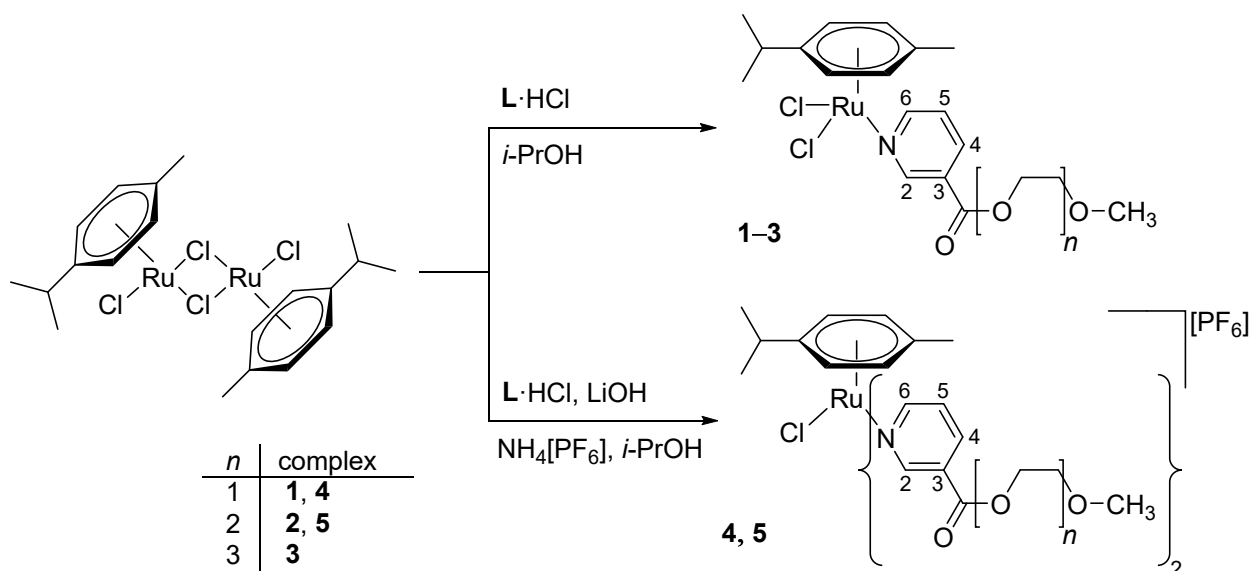
^1H			^{13}C		
H Atom	Exp. (ppm)	Calc. (ppm)	C Atom	Exp. (ppm)	Calc. (ppm)
OCH ₃	3.34	3.53	CH ₃ O	58.0	57.9
CH ₃ OCH ₂ CH ₂	3.79	3.78	CH ₂ OOC	65.7	68.2
OOCCH ₂ CH ₂	3.97	4.01	CH ₂ O	68.2	69.1
COOCH ₂	4.66	4.61	CH ₂ O	69.5	72.4
C5-H	8.28	8.44	CH ₂ O	70.9	73.4
C4-H	9.06	8.88	C5	127.7	127.0
C6-H	9.18	9.30	C3	129.7	132.2
C2-H	9.44	10.00	C2	142.7	141.2
R		0.997	C4	144.5	141.4
MAE (ppm)		0.16	C6	147.1	148.8
			COO	162.9	158.6
			R		0.999
			MAE (ppm)		1.0

Regarding ^{13}C NMR chemical shifts, the correlation coefficient and MAE parameters for comparing theoretical and experimental values are 0.999 and 1.0 ppm. The lowest values were obtained for the carbon atoms of the aliphatic chain, between 58.0 and 70.9 ppm (experimental) and between 57.9 and 73.4 ppm (theoretical). These values gradually increase with the proximity of the ester group. The aromatic carbon atoms have chemical shifts between 127.7 and 147.1 ppm, depending on the distance from the nitrogen atom and carboxyl group. The value of 162.9 ppm is obtained for the carbon atom of the ester group, which is expected due to the electronegativity of oxygen atoms. In the theoretical spectrum, the resonance of carbon atoms from the ester group is located at 158.6 ppm. Again, these experimental values are almost identical for all three ligands, proving the assumption that the elongation of the aliphatic chain does not influence the magnetic environment of the neighboring atoms significantly.

The structures of ligand precursors are stabilized by various intramolecular interactions. The most important stabilization interactions of **L2**·HCl from the second-order perturbation theory analysis are discussed within this paragraph. As previously observed, the strongest interactions are formed within the pyridine ring and carboxylic group, leading to the planarity of this part of a molecule. The interactions denoted as $\pi(\text{C}-\text{C}) \rightarrow \pi^*(\text{C}-\text{C})$ have stabilization energies of 66–105 kJ mol⁻¹. Bonds that include nitrogen atom are also very important for stabilizing the ring structure. They are included in the following stabilization interactions: $\pi(\text{C}-\text{C}) \rightarrow \pi^*(\text{C}-\text{N})$ (67–123 kJ mol⁻¹), $\pi(\text{C}-\text{C}) \rightarrow \pi^*(\text{C}-\text{C})$ (50–113 kJ mol⁻¹), and $\text{LP}(\text{N}) \rightarrow \pi^*(\text{C}-\text{C})$ (38 kJ mol⁻¹). An electron delocalization can be observed at the intersection between the pyridine ring and aliphatic chain, represented by a stabilization interaction with an energy of 10 kJ mol⁻¹. The ester group is stabilized by interactions denoted as $\text{LP}(\text{O}) \rightarrow \pi^*(\text{C}-\text{O})$ (196 kJ mol⁻¹) and $\text{LP}(\text{O}) \rightarrow \sigma^*(\text{C}-\text{O})$ (133 kJ mol⁻¹). The other oxygen atoms stabilize the neighboring C–C moieties by donating the free electron pair. Except for the increased number of stabilization interactions, there are no differences in their strength with the elongation of the aliphatic chain in ligands **L1**·HCl to **L3**·HCl.

2.3. Synthesis and Characterization of Neutral $[\text{RuCl}_2(\eta^6\text{-}p\text{-cym})(\text{L}-\kappa\text{N})]$ ($\text{L} = \text{L2: 2; L3: 3}$) Complexes

Complexes **2** and **3** were prepared using a procedure described in the literature [31,32], while complex **1** was previously reported [29]. The starting Ru(II) dimer was dissolved in *iso*-propanol and the appropriate ligand precursor, $\text{L2}\cdot\text{HCl}$ or $\text{L3}\cdot\text{HCl}$, was added (Scheme 2). The yellow or orange products were isolated in high yields (**2**: 96%; **3**: 90%)



Scheme 2. Preparation of $[\text{RuCl}_2(\eta^6\text{-}p\text{-cym})(\text{L}-\kappa\text{N})]$ and $[\text{RuCl}(\eta^6\text{-}p\text{-cym})(\text{L}-\kappa\text{N})_2][\text{PF}_6]$ complexes ($\text{L} = \text{L1: 1, 4; L2: 2, 5; L3: 3}$).

The prepared complexes were also studied via ESI-HRMS in a methanolic solution. Appropriate ions of complexes **2** and **3** were detected in a positive mode. Due to the presence of chlorine and ruthenium atoms, the spectra show a characteristic isotopic pattern. The obtained m/z ions for **2** and **3** were found at 490.08585 and 534.11190, respectively. These values reproduce well the calculated ones of 490.08556 (**2**, deviation 0.6 ppm) and 534.11178 (**3**, deviation 0.2 ppm). The elemental analysis proved the purity of the obtained compounds.

The NMR spectra of both complexes show similar patterns. The lowest values of the chemical shifts in ^1H NMR spectra were found, as expected, for the *iso*-propyl and methyl groups belonging to the *p*-cymene moiety (1.32 ($\text{CH}(\text{CH}_3)_2$), 2.13 (CCH_3), and 2.99 ppm ($\text{CH}(\text{CH}_3)_2$)), as described previously in the literature [29,33]. The chemical shifts originating from the polyethylene oxide spacers are located between 3.38 and 5.46 ppm, depending on the proximity of the electronegative oxygen atoms. It should be mentioned that the size of the back chain does not influence the resonance of hydrogen atoms significantly, as observed for $\text{L2}\cdot\text{HCl}$ and $\text{L3}\cdot\text{HCl}$ ligand precursors. Chemical shifts assigned to the pyridine hydrogen atoms are found between 7.41 and 9.63 ppm. Protons of the *p*-cymene ligand are allocated between 5.2 and 5.5 ppm, which is in accordance with the literature data [29]. The formation of the Ru–N bond in complexes induces a change in the magnetic surrounding of the pyridine protons by creating a strong downfield. The chemical shifts of protons in the *ortho*-position in the pyridine ring have resonances at 9.6 ppm with a coordination-induced shift of 0.2 ppm. For the other hydrogen atoms, from the alkyl chain, the resonances remained almost unchanged upon the complexation of the ligand. In the ^{13}C NMR spectra, chemical shifts between 18.4 and 30.8 ppm are assigned to sp^3 -hybridized carbon atoms (Me and *i*-Pr groups) of the *p*-cymene moiety. The resonances belonging to the carbon atoms of the polyethylene glycol pendant groups, in the area between 59.2 and 75 ppm, remained the same upon the complexation of the pyridine moiety. The most notable differences were observed for the carbon atoms in the vicinity of

the nitrogen atom bound to ruthenium(II). These changes are around 13 ppm, which proves that the coordination occurred through the pyridine nitrogen atom. Further evidence of nitrogen coordination was obtained with the $^1\text{H},^{13}\text{C}$ -COSY spectrum (Figure 2). For the carbon atoms, numerated as B and E (Figure 2), resonances are found at approximately 97 and 107 ppm in the ^{13}C NMR spectra and could not be assigned to one particular atom. In contrast, the carbon atoms C and D are found closely together at 82 and 83 ppm and could be assigned due to measured $^1\text{H},^1\text{H}$ - and $^{13}\text{C},^1\text{H}$ -COSY NMR experiments, which allowed resonances of the *p*-cymene moiety to be assigned to these hydrogen and carbon atoms due to an observed correlation between the protons of the methyl group (A) and both aromatic protons near to the methyl protons (C).

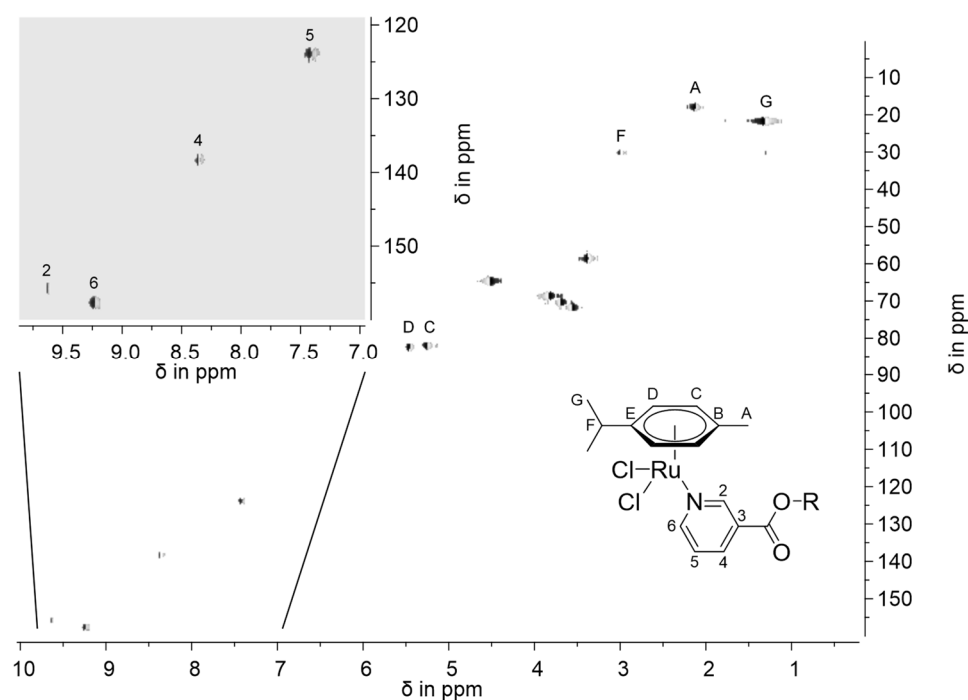


Figure 2. $^{13}\text{C},^1\text{H}$ -COSY NMR spectra of **2** (400 MHz, CDCl_3).

The IR spectra of complexes **2** and **3** show several characteristic vibrations for the coordinated ligands. Bands at 3088 and 3026 in the spectrum of **2** and 3065 cm^{-1} in the spectrum of **3** are assigned to the C–H vibrations of the aromatic and pyridine moieties. Bands below 3000 cm^{-1} belong to the C–H vibrations of the aliphatic chain. The carbonyl group stretching vibration is observed as a strong band at 1724 (**2**) and 1722 (**3**), almost unchanged compared to the ligand precursors. These values also prove that their position is not dependent on the number of polyethylene glycol bridging groups. The same applies to the strong bands at 1280 and 1105 cm^{-1} assigned to single carbon–oxygen bonds. A strong band at 750 cm^{-1} originating from pyridine ring vibrations also remains unchanged. One noticeable difference between the ligand precursors and the complex is the appearance of the strong band at 285 cm^{-1} , which represents Ru–Cl stretching vibration. These positions and relative intensities are shared with **1**, as previously described [29].

2.4. Theoretical Analysis of Neutral $[\text{RuCl}_2(\eta^6\text{-}p\text{-cym})(\text{L}-\kappa\text{N})]$ ($\text{L} = \text{L1: 1; L2: 2; L3: 3}$) Complexes

The structures of neutral complexes were optimized at the B3LYP/6-31+G(d,p)(H,C,N,O,Cl)/LanL2DZ(Ru) level of theory, as it was shown that this level of theory could be used for the description of the structure and spectral assignment of similar compounds [33,34]. Figure 3 represents an optimized structure of **2** as an example of this class of compounds. It can be assumed that there are no significant differences between this compound and analogous complexes containing **L1** and **L3**. Complex **2** consists of two chlorido, the *p*-

cymene group, and L2 ligands. These ligands form a half-sandwich complex in which three facial positions are occupied by *p*-cymene through π -bonding. The optimized bond distance between Ru(II) and chlorido ligands is 2.43 Å, within the range obtained from similar compounds' crystallographic and optimized structures [33,35,36]. Ru–C (*p*-cymene) distances are between 2.23 and 2.29 Å, a common range for the complexes in the half-sandwich structures [33,35]. The bond length between Ru(II) and nitrogen is 2.15 Å, similar to the experimental found values, e.g., within the Ru(II)-1-Naphthylhydrazine complex [33]. Also, the bond distances are very close for all three complexes (1–3), which is expected as the added monomers of ethylene glycol esters do not influence these interactions. The bond angle between chlorido ligands and Ru(II) is 89.4°, while N–Ru–Cl angles are 84.7 and 86.9°. These values show that a pseudo-octahedral geometry of the complex is formed. The optimized structure was further used to univocally assign NMR chemical shifts.

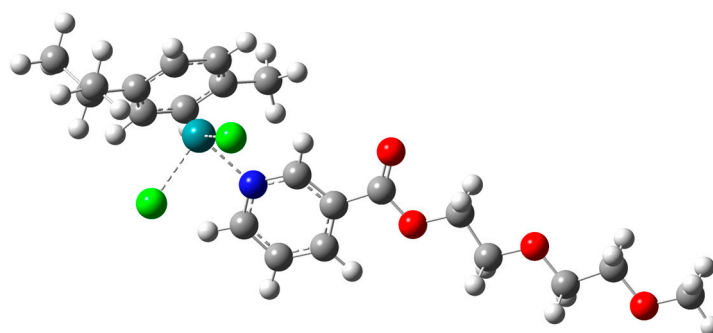


Figure 3. Optimized structure of 2 at B3LYP/6-31+G(d,p) level of theory (hydrogen—white, carbon—gray, nitrogen—blue, oxygen—red, chlorine—green, ruthenium—teal).

The theoretical NMR spectra of complex 2 show high correlation coefficients (0.997) and low MAE values (0.32 and 3.6 ppm) when compared to the experimental ones (Table 2). The obtained ^1H NMR chemical shifts lie in their expected range. Much more important is the fact that calculation allowed for the assignment of resonances in ^{13}C NMR spectra, especially for those carbon atoms that are in similar magnetic surroundings. This is true for carbon atoms of the polyethylene glycol ester part of the molecule, with chemical shifts between 61.0 and 74.5 ppm. Two groups of carbon atoms in the *p*-cymene moiety that have similar chemical shifts in the experimental spectrum (82.5 and 82.8 ppm) have a much more pronounced difference in the theoretical spectrum (83.7 and 92.9 ppm), probably due to the overall geometry of the complex and shorter distance between carbon atoms and Ru(II). The carbon atom attached to the *iso*-propyl group, previously denoted as E, is assigned to the chemical shift of 97.4 ppm in the experimental spectrum and 102.7 ppm in the theoretical spectrum. On the other side, the carbon atom in position B has higher shifts of 103.9 and 106.1 ppm in the experimental and theoretical spectra, respectively. As for the rest of the carbon atoms, these two sets of values differ up to 3 ppm, which is acceptable difference.

Table 2. Experimental and theoretical (at B3LYP/6-31+G(d,p) level of theory) ^1H and ^{13}C NMR chemical shifts of **2**.

^1H			^{13}C		
H Atom	Exp. (ppm)	Calc. (ppm)	C Atom	Exp. (ppm)	Calc. (ppm)
CH(CH ₃) ₂	1.32	2.12	CCH ₃	18.4	22.0
CCH ₃	2.13	2.44	C(CH ₃) ₂	22.4	25.7
CH(CH ₃) ₂	2.99	3.75	C(CH ₃) ₂	30.8	40.4
OCH ₃	3.38	3.87	CH ₃ O	59.2	61.0
CH ₃ OCH ₂	3.57	3.92	CH ₂ OOC	65.3	68.3
CH ₃ OCH ₂ CH ₂	3.70	4.04	CH ₂ CH ₂ OOC	69.5	71.9
COOCH ₂ CH ₂	3.84	4.15	CH ₃ OCH ₂ CH ₂	70.8	73.9
COOCH ₂	4.53	4.56	CH ₃ OCH ₂	72.1	74.5
CHCCH ₃	5.25	5.09	CH ₃ CCH	82.5	83.7
CHCHCCH ₃	5.46	5.58	CH ₃ CCHCH	82.8	92.9
C5-H	7.41	7.23	CCH(CH ₃) ₂	97.4	102.7
C4-H	8.35	8.13	CCH ₃	103.9	106.1
C6-H	9.23	8.97	C5	124.2	121.0
C2-H	9.63	9.36	C3	127.4	126.5
R		0.997	C4	138.7	134.9
MAE (ppm)		0.32	C2	156.3	151.8
			C6	158.0	155.0
			COO	163.6	161.7
			R		0.997
			MAE (ppm)		3.6

The NBO analysis of the complexes was used to quantify the intramolecular interactions. The importance of the *p*-cymene moiety for the overall stability of the complex can be seen in the interactions between $\pi(\text{C}-\text{C})$ orbitals and empty Ru(II) orbitals, with stabilization energy up to 400 kJ mol^{-1} . Various stabilization interactions between a lone pair of chlorine and empty orbitals of ruthenium(II) were found, with stabilization energies between 78 and 367 kJ mol^{-1} , depending on the orientation of the orbital. In contrast, interactions denoted as $\text{LP}(\text{Ru}) \rightarrow \text{LP}^*(\text{Cl})$ are much weaker, below 12 kJ mol^{-1} . The electron donation from the nitrogen atom of the pyridine moiety can be present through $\text{LP}(\text{N}) \rightarrow \text{LP}^*(\text{Ru})$ with an energy of 422 kJ mol^{-1} . Carbon–nitrogen bonds also stabilize the system through $\pi(\text{C}-\text{N}) \rightarrow \text{LP}^*(\text{Ru})$ (17 – 39 kJ mol^{-1}). It has been shown that the formation of complexes does not affect the interactions within the ligand structure [33,34]; therefore, they are not explicitly listed herein. These interactions verify the donation of surrounding ligands to the Ru(II) ion and their effects on stability.

2.5. Synthesis and Structural Characterization of Cationic $[\text{RuCl}(\eta^6\text{-p-cym})(\text{L}-\kappa\text{N})_2][\text{PF}_6]$ (**L** = **L1**: **4**; **L2**: **5**) Complexes

The cationic ruthenium(II) complexes were obtained from a ruthenium(II) dimer and appropriate ligand precursor in the presence of base (LiOH) and $\text{NH}_4[\text{PF}_6]$ (Scheme 2). The reaction was monitored using ^1H NMR spectroscopy, and a fast formation of the cationic complex was observed, although this product was not stable and reacted back to **1** (Figure 4c). A small amount of lithium hydroxide was added to the mixture, and the reaction progress was monitored using ^1H NMR spectroscopy. The last step was repeated until the whole neutral complex was consumed (Figure 4d). The same procedure was applied for the preparation of complex **5**, which contains two **L2** ligands. Complexes **4** and **5** were highly viscous oils, soluble in chloroform and dichloromethane.

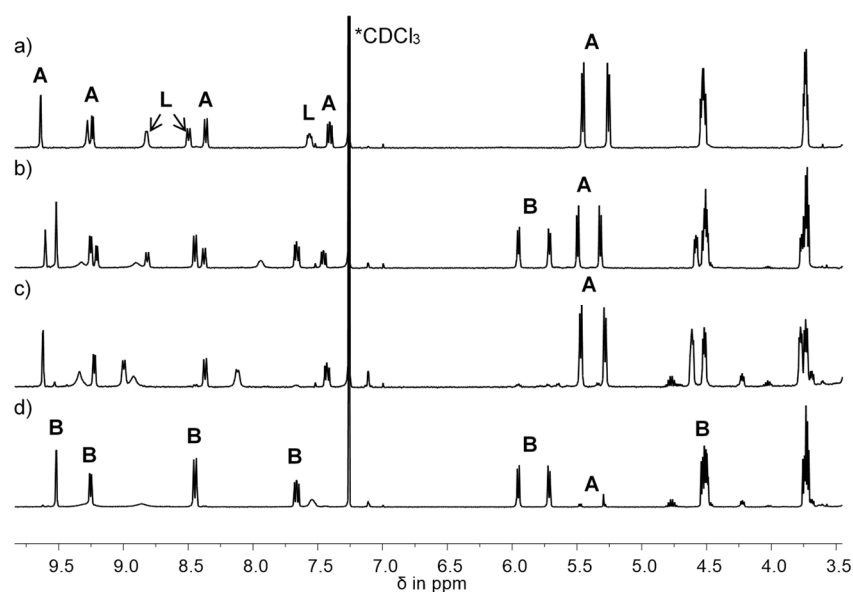


Figure 4. ^1H NMR spectra (400 MHz, CDCl_3) of the synthesis of **4**: (a) neutral complex **1** (A); (b) cationic and neutral complex after addition of $\text{NH}_4[\text{PF}_6]$; (c) back reaction to neutral complex **1** (A); (d) nearly completed reaction, cationic complex **4** (B).

Both complexes **4** and **5** were characterized via multinuclear NMR spectroscopy (^1H , ^{13}C , and ^{31}P). Resonances of the poly(ethylene oxide) pendant moiety in ^1H and ^{13}C NMR spectra of cationic complexes **4** and **5** do not differ significantly from appropriate neutral complexes **1** and **2**. The most apparent change in ^1H NMR spectra was observed for the *p*-cymene ligand. The resonances of all non-aromatic protons of the *p*-cymene ligand are shifted to a higher field, and both prepared cationic ruthenium(II) complexes show the same chemical shifts. Also, the coupling constants of the aromatic ligand remained unchanged. All proton resonances of the nicotinate group are slightly shifted and could be assigned. The obtained ^{13}C NMR spectra also show the prominent changes in the resonances for the aromatic carbon atoms from the *p*-cymene moiety. All other chemical shifts are found at nearly the same frequency positions as in the neutral complexes. The resonances of *ipso*-carbon atoms are located close to each other in cationic complexes **4** and **5** at approximately 102 and 103 ppm. Other carbon atoms of the *p*-cymene are shifted to lower field at 82.5 and 88.5 ppm. All other resonances are assigned at their expected frequencies and are only slightly changed. A septet, a chemical shift found in ^{31}P NMR spectra, was at -144.2 ppm, the value expected for phosphorus in the hexafluorophosphate anion [29]. The infrared spectrum of **4** shows all four characteristic bands of the ligands and an additional 290 cm^{-1} belonging to Ru–Cl vibrations. The strongest band is found at 1290 cm^{-1} and is assigned to the carbon–oxygen vibrations of the ester group. A band at 837 cm^{-1} is stronger than the band at 746 cm^{-1} and is assigned to the stretching vibrations of the hexafluorophosphate anion [37].

2.6. Theoretical Analysis of Cationic $[\text{RuCl}(\eta^6\text{-}p\text{-cym})(\text{L}-\kappa\text{N})_2][\text{PF}_6]$ (L = L1: **4**; L2: **5**) Complexes

The structures of complexes containing two L1 or L2 ligands were optimized at the B3LYP/6-31+G(d,p) level of theory. Their structures are shown in Figure 5, with hydrogen atoms omitted for clarity. When Ru–Cl bonds are concerned, their lengths are 2.42 (**4**) and 2.43 Å (**5**), almost identical to the previously described neutral complexes. The distances between Ru(II) and aromatic carbon atoms of the *p*-cymene moiety are between 2.28 and 2.35 Å. These values are slightly higher than those for neutral complexes, probably due to the repulsion between pyridine ligands and the *p*-cymene moiety. The Ru–N distances are equal in both complexes (2.15 and 2.17 Å), proving that the length of the poly(ethylene oxide) ligand does not affect the geometry of the complex. This value is also identical to the

Ru(II)-1-naphthylhydrazine complex, as determined experimentally [33]. Because of the presence of ether groups, some of the ligands within the structure were twisted, which can be expected due to the formation of weak interactions between chains. The angles formed between the chlorido ligand, Ru(II), and nitrogen atoms are 84° and 88° , a further deviation from the octahedral structure. The angle N(py)–Ru–N(py) is 89° , close to the ideal value of 90° in octahedral geometry. These changes in angles can be attributed to the formed stabilization interactions, as presented below.

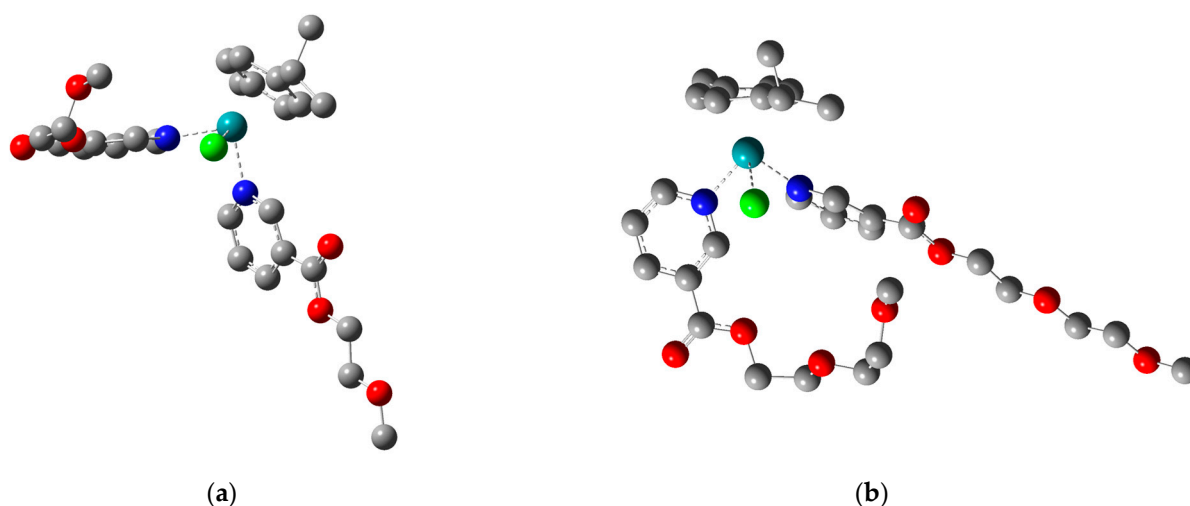


Figure 5. Optimized structures of (a) 4 and (b) 5 at B3LYP/6-31+G(d,p) level of theory (carbon—gray, nitrogen—blue, oxygen—red, chlorine—green, ruthenium—teal; hydrogen atoms are omitted for clarity).

The most numerous interactions are formed between *p*-cymene and Ru(II), denoted as $\pi(\text{C}-\text{C}) \rightarrow \text{LP}^*(\text{Ru})$ ($67\text{--}368 \text{ kJ mol}^{-1}$). The interactions between the chlorido ligand and Ru(II) are much stronger, with stabilization energies up to 576 kJ mol^{-1} . This change was expected because of the overall charge of the complex. The interactions between the nitrogen atom of pyridine and Ru(II) are around 334 kJ mol^{-1} . These values are weaker than those previously discussed, resulting from the presence of two neutral and voluminous ligands. Because of these stability parameters, it would be beneficial to examine the effect of these changes on biological activity in future research.

3. Materials and Methods

3.1. Purchased Chemicals

Nicotinic acid, dimethylformamide, and thionyl chloride were obtained from Acros Organics. Toluene, acetone, acetonitrile, diethyl ether, dichloromethane, ammonium hexafluoride phosphate, lithium hydroxide, and a dichlorido(η^6 -*p*-cym)ruthenium(II) dimer were ordered from Merck.

3.2. Preparative Technique and Instrumental Methods

All three ligands were prepared in dry toluene and acetonitrile. Corresponding ruthenium(II) compounds were synthesized under nitrogen using the standard Schlenk line technique. Sodium benzophenone was removed from diethyl ether and toluene via distillation. Dichloromethane was distilled from calcium hydride. 2-Propanol was dried with molecular sieve 3 \AA and degassed with argon prior to use. Ethylene glycol was freshly distilled and stored with molecular sieve 4 \AA . All other poly(ethylene oxide) compounds and poly(ethylene oxide) monomethyl ethers were dried with sodium sulfate.

The NMR spectra were obtained on a Varian Unity 400 or Varian Gemini 400 spectrometers in 5 mm NMR tubes at 300 K. The chemical shifts in ^1H NMR spectra are shown

relative to undeuterated solvents, $CHCl_3$ (δ 7.26) and HDO (δ 4.79). On the other side, ^{13}C NMR chemical shifts are calibrated to $CDCl_3$ (δ 77.16) or for D_2O with tetramethylsilane (TMS). The IR spectra were recorded from 4000 to 250 cm^{-1} on a Bruker Tensor 27 FT-IR spectrometer with diamond ATR. The high-resolution ESI spectra of the compounds were measured on Bruker Apex III Fourier transform ion cyclotron resonance (FTR-ICR) mass spectrometers (Bruker Daltonics) equipped with an Infinity cell, a 7.0 T superconducting magnet (Bruker), an rf-only hexapole ion guide, and an external APOLLO electrospray ion source (Agilent, off-axis spray). The sample solutions were introduced continuously via a syringe pump with a flow rate of $120\ \mu\text{L}\cdot\text{h}^{-1}$. Ligand precursors are noted without hydrochloride as $[M + H]^+$. The electronic spectra were prepared on an HP 8453 at RT and in quartz cuvettes from Hellma GmbH & Co. with sides of 1 cm.

3.3. Preparation of Ligands

Nicotinic acid and dimethylformamide (0.03 g, 0.4 mmol) were cooled to $15\text{ }^\circ\text{C}$, and excess thionyl chloride (5 mL, 70 mmol) was added dropwise. The reaction mixture was stirred at $40\text{ }^\circ\text{C}$ for 1 h. The formed light yellow acyl chloride hydrochloride was obtained by evaporating the solvent and the rest of the thionyl chloride and dried in vacuo. The obtained acyl chloride hydrochloride was used in situ to prepare poly(ethylene glycol) esters. The acyl chloride hydrochloride was suspended in toluene (40 mL). The appropriate poly(ethylene oxide) monomethyl ether was added at $15\text{ }^\circ\text{C}$ and stirred overnight at rt. Viscous oils were obtained, toluene was removed in vacuo, and impurities were removed via extraction with acetone/diethyl ether.

L2·HCl (2-(2-Methoxyethoxy)ethyl nicotinate hydrochloride): Viscous, hygroscopic oil; soluble in water, methanol, ethanol, and *iso*-propanol; insoluble in diethyl ether. Yield: 95%. $^1\text{H-NMR}$ (400 MHz, D_2O): δ 3.34 (s, 3H, OCH_3), 3.66, 3.79 (m, 4H, $CH_3OCH_2CH_2$), 3.97 (m, 2H, $OOCCH_2CH_2$), 4.66 (m, 2H, $COOCH_2$), 8.28 (ddd, $^3J_{H_5,H_6} = 8.2\text{ Hz}$, $^3J_{H_5,H_4} = 5.9\text{ Hz}$, $^4J_{H_5,H_2} = 0.8\text{ Hz}$, 1H, H^5), 9.06 (d(b), $^3J_{H,H} = 5.9\text{ Hz}$, 1H, H^4), 9.18 (d(b), $^3J_{H,H} = 8.2\text{ Hz}$, 1H, H^6), 9.44 (m, 1H, H^2). $^{13}C\text{-NMR}$ (100 MHz, D_2O): δ 58.0 (CH_3O), 65.7 (CH_2OOC), 68.2, 69.5, 70.9 (CH_2O), 127.7 (C^5), 129.7 (C^3), 142.7 (C^2), 144.5 (C^4), 147.1 (C^6), 162.9 (COO). ESI-HRMS (CH_3OH), positive mode: Calcd for $[C_{11}H_{16}NO_4]^+$ 226.10738, m/z 226.10733 $[M + H]^+$. IR: ν (cm^{-1}) 3061(w), 2876(w), 2400(b), 2090(w), 1968(w), 1728(s), 1633(w), 1606(w), 1544(w), 1461(m), 1359(w), 1286(s), 1198(w), 1103(s), 1019(m), 928(w), 837(w), 740(s), 690(m), 677(m), 619(s), 520(w), 469(w).

L3·HCl (2-[2-(2-Methoxyethoxy)ethoxy]ethyl nicotinate hydrochloride): Viscous, hygroscopic oil; soluble in water, methanol, ethanol, *iso*-propanol, chloroform, and dichloromethane; insoluble in diethyl ether. Yield: 92%. $^1\text{H-NMR}$ (400 MHz, D_2O): δ 3.33 (s, 3H, OCH_3), 3.58, 3.66, 3.69, 3.78 (m, 8H, OCH_2CH_2O), 3.95 (m, 2H, $OOCCH_2CH_2$), 4.63 (m, 2H, $COOCH_2$), 8.27 (dd, $^3J_{H_5,H_6} = 8.2\text{ Hz}$, $^3J_{H_5,H_4} = 6.0\text{ Hz}$, 1H, H^5), 9.05 (d(b), $^3J_{H,H} = 5.9\text{ Hz}$, 1H, H^4), 9.17 (d(b), $^3J_{H,H} = 8.2\text{ Hz}$, 1H, H^6), 9.43 (s(b), 1H, H^2). $^{13}C\text{-NMR}$ (100 MHz, D_2O): δ 58.0 (CH_3O), 65.7 (CH_2OOC), 68.2, 69.4, 69.4, 69.7, 70.9 (CH_2O), 127.7 (C^5), 129.7 (C^3), 142.7 (C^2), 144.5 (C^4), 147.1 (C^6), 162.9 (COO). ESI-HRMS (CH_3OH), positive mode: Calcd for $[C_{13}H_{20}NO_5]^+$ 270.13360, m/z 270.13355 $[M + H]^+$. IR: ν (cm^{-1}) 3065(w), 2876(w), 2400(b), 2092(w), 1970(w), 1730(s), 1633(w), 1606(w), 1540(w), 1461(m), 1355(w), 1286(s), 1198(w), 1100(s), 1016(m), 935(w), 837(m), 740(s), 695(m), 677(m), 619(s), 520(w), 479(w).

3.4. Preparation of $[RuCl_2(\eta^6\text{-}p\text{-cym})(L-\kappa N)]$ Complexes (L = L2: 2; L3: 3)

The appropriate ligand precursor (0.22 mmol) was suspended in *iso*-propanol (20 mL) and stirred at rt. A dichlorido($\eta^6\text{-}p\text{-cymene}$)ruthenium(II) dimer was added, and the orange reaction mixture was heated to $40\text{ }^\circ\text{C}$ and stirred for 1 h. The suspension turned light orange or yellow and was cooled to $-47\text{ }^\circ\text{C}$. The product was precipitated and filtered off, washed with diethyl ether ($4 \times 2\text{ mL}$), and dried in air.

2: Orange powder; soluble in chloroform, dichloromethane, dimethylformamide, acetone, and acetonitrile; moderately soluble in methanol, ethanol, *iso*-propanol, and tetrahydrofuran; insoluble in diethyl ether and toluene. Yield: 96%. EA: Anal. Found: C, 47.03; H,

5.19; N, 2.62. Calcd for $C_{21}H_{29}Cl_2NO_4Ru$ (531.43): C, 47.46; H, 5.50; N, 2.64. 1H -NMR (400 MHz, $CDCl_3$): δ 1.32 (d, $^3J_{H,H} = 7.2$ Hz, 6H, $CH(CH_3)_2$), 2.13 (s, 3H, CCH_3), 2.99 (sept, $^3J_{H,H} = 6.9$ Hz, 1H, $CH(CH_3)_2$), 3.38 (s, 3H, OCH_3), 3.57, 3.70 (m, 4H, $CH_3OCH_2CH_2$), 3.84 (m, 2H, $OOCCH_2CH_2$), 4.53 (m, 2H, $COOCH_2$), 5.25 (d, $^3J_{H,H} = 6.0$ Hz, 2H, $CHCCH_3$), 5.46 (d, $^3J_{H,H} = 5.9$ Hz, 2H, $CHCHCCH_3$), 7.41 (dd, $^3J_{H_5,H_4} = 7.8$ Hz, $^3J_{H_5,H_6} = 5.7$ Hz, 1H, H^5), 8.35 (d, $^3J_{H,H} = 7.9$ Hz, 1H, H^4), 9.23 (d, $^3J_{H,H} = 5.6$ Hz, 1H, H^6), 9.63 (s, 1H, H^2). ^{13}C -NMR (100 MHz, $CDCl_3$): δ 18.4 (CCH_3), 22.4 ($C(CH_3)_2$), 30.8 ($C(CH_3)_2$), 59.2 (CH_3O), 65.3 (CH_2OOC), 69.0, 70.8, 72.1 (CH_2O), 82.5, 82.8 (CH), 97.4, 103.9 (CCH), 124.2 (C^5), 127.4 (C^3), 138.7 (C^4), 156.3 (C^2), 158.0 (C^6), 163.6 (COO). ESI-HRMS (CH_3OH), positive mode: Calcd for $[C_{21}H_{29}ClNO_4^{96}Ru]^+$ 490.08556, m/z 490.08585 $[M-Cl]^+$. IR: ν (cm^{-1}) 3088(w), 3026(w), 2968(w), 2880(w), 1724(s), 1604(w), 1469(w), 1451(w), 1428(w), 1381(w), 1353(w), 1319(w), 1286(s), 1250(m), 1202(w), 1144(m), 1111(s), 1053(m), 1016(m), 944(m), 881(m), 845(m), 802(w), 751(s), 695(m), 670(w), 528(w), 500(w), 470(w), 455(w), 371(w), 287(s), 269(s), 229(s).

3: Orange powder; soluble in chloroform, dichloromethane, dimethylformamide, acetone, and acetonitrile; moderately soluble in methanol, ethanol, *iso*-propanol, and tetrahydrofuran; insoluble in diethyl ether and toluene. Yield: 90%. EA: Anal. Found: C, 47.85; H, 5.41; N, 2.40. Calcd for $C_{23}H_{33}Cl_2NO_5Ru$ (575.49): C, 48.00; H, 5.78; N, 2.43. 1H -NMR (400 MHz, $CDCl_3$): δ 1.32 (d, $^3J_{H,H} = 6.9$ Hz, 6H, $CH(CH_3)_2$), 2.13 (s, 3H, CCH_3), 2.99 (sept, $^3J_{H,H} = 6.9$ Hz, 1H, $CH(CH_3)_2$), 3.36 (s, 3H, OCH_3), 3.54, 3.64, 3.69, 3.71 (m, 8H, $CH_3OCH_2CH_2$), 3.84 (m, 2H, $OOCCH_2CH_2$), 4.52 (m, 2H, $COOCH_2$), 5.26 (d, $^3J_{H,H} = 6.0$ Hz, 2H, $CHCCH_3$), 5.46 (d, $^3J_{H,H} = 6.0$ Hz, 2H, $CHCHCCH_3$), 7.41 (dd, $^3J_{H_5,H_4} = 7.8$ Hz, $^3J_{H_5,H_6} = 5.8$ Hz, 1H, H^5), 8.35 (d, $^3J_{H,H} = 7.9$ Hz, 1H, H^4), 9.23 (d, $^3J_{H,H} = 5.6$ Hz, 1H, H^6), 9.62 (s, 1H, H^2). ^{13}C -NMR (100 MHz, $CDCl_3$): δ 18.4 (CCH_3), 22.4 ($C(CH_3)_2$), 30.8 ($C(CH_3)_2$), 59.2 (CH_3O), 65.3 (CH_2OOC), 69.0, 70.7, 70.8, 70.9, 72.1 (CH_2O), 82.5, 82.8 (CH), 97.4, 103.9 (CCH), 124.2 (C^5), 127.5 (C^3), 138.7 (C^4), 156.3 (C^2), 158.0 (C^6), 163.6 (COO). ESI-HRMS (CH_3OH), positive mode: Calcd for $[C_{23}H_{33}ClNO_5^{96}Ru]^+$ 534.11178, m/z 534.11190 $[M-Cl]^+$. IR: ν (cm^{-1}) 3065(w), 2964(w), 2877(w), 1722(s), 1600(w), 1472(w), 1451(w), 1428(w), 1380(w), 1282(s), 1198(m), 1105(s), 1053(m), 1028(m), 947(w), 867(m), 845(m), 798(w), 751(s), 693(m), 455(w), 371(w), 284(s), 232(s).

3.5. Preparation of $[RuCl(\eta^6-p-cym)(L-\kappa N)_2][PF_6]$ (**L** = **L1**: **4**; **L2**: **5**) Complexes

The appropriate ligand precursor (**L1**·HCl: 0.48 mmol; **L2**·HCl: 0.43 mmol) was suspended in *iso*-propanol (20 mL), and lithium hydroxide (1 eq) was added. The suspension was stirred for 1 h at 40 °C. A dichlorido(η^6 -*p*-cymene)ruthenium(II) dimer (0.075 mmol) was added, and the orange reaction mixture was stirred for 2 h and cooled afterward to rt. Dichloromethane was added until the precipitated neutral ruthenium(II) complex was redissolved. Excess ammonium hexafluoridophosphate (1.5 mmol) was added in one portion, and the rest of the lithium hydroxide (**4**: overall 0.90 mmol; **5**: overall 0.59 mmol) was added in small portions under stirring over 4 h. The crude product precipitated from the reaction mixture at -70 °C and was separated and redissolved in small amounts in dichloromethane, and the byproducts were filtered off. The product was then obtained via the evaporation of dichloromethane and dried in air.

4: Orange, highly viscous oil; soluble in chloroform and dichloromethane; moderately soluble in methanol, ethanol, and *iso*-propanol; insoluble in *n*-pentane. Yield: 19%. 1H -NMR (400 MHz, $CDCl_3$): δ 1.16 (d, $^3J_{H,H} = 6.9$ Hz, 6H, $CH(CH_3)_2$), 1.77 (s, 3H, CCH_3), 2.59 (sept, $^3J_{H,H} = 6.9$ Hz, 1H, $CH(CH_3)_2$), 3.38 (s, 6H, OCH_3), 3.70 (t, $^3J_{H,H} = 4.7$ Hz, 4H, OCH_2), 4.48 (m, 4H, $COOCH_2$), 5.69 (d, $^3J_{H,H} = 6.1$ Hz, 2H, $CHCCH_3$), 5.94 (d, $^3J_{H,H} = 6.1$ Hz, 2H, $CHCHCCH_3$), 7.65 (dd, $^3J_{H_5,H_4} = 7.8$ Hz, $^3J_{H_5,H_6} = 5.8$ Hz, 2H, H^5), 8.43 (d, $^3J_{H,H} = 8.0$ Hz, 2H, H^4), 9.21 (d, $^3J_{H,H} = 5.6$ Hz, 2H, H^6), 9.47 (s, 2H, H^2). ^{13}C -NMR (100 MHz, $CDCl_3$): δ 18.0 (CCH_3), 22.3 ($C(CH_3)_2$), 31.0 ($C(CH_3)_2$), 59.1 (CH_3O), 65.3 (CH_2OOC), 70.2 (CH_2O), 82.5, 88.5 (CH), 102.1, 103.4 (CCH), 126.7 (C^5), 128.6 (C^3), 140.2 (C^4), 154.4 (C^2), 158.5 (C^6), 163.2 (COO). ^{31}P -NMR (162 MHz, $CDCl_3$): δ -144.2 (sept, $J_{P,F} = 713$ Hz, PF_6) IR: ν (cm^{-1})

3080(w), 2968(w), 2887(w), 1726(s), 1606(w), 1433(w), 1369(w), 1290(s), 1197(w), 1118(m), 1055(w), 1026(w), 837(s), 746(m), 694(w), 557(m), 293(w).

5: Orange, highly viscous oil; soluble in chloroform and dichloromethane; moderately soluble in methanol, ethanol, and *iso*-propanol; insoluble in *n*-pentane. Yield: 39%. ¹H-NMR (400 MHz, CDCl₃): δ 1.17 (d, ³J_{H,H} = 6.9 Hz, 6H, CH(CH₃)₂), 1.78 (s, 3H, CCH₃), 2.58 (sept, ³J_{H,H} = 7.0 Hz, 1H, CH(CH₃)₂), 3.35 (s, 6H, OCH₃), 3.56, 3.69, 3.84 (m, 12H, OCH₂), 4.53 (m, 4H, COOCH₂), 5.71 (d, ³J_{H,H} = 6.1 Hz, 2H, CHCCH₃), 5.95 (d, ³J_{H,H} = 6.1 Hz, 2H, CHCHCCH₃), 7.66 (dd, ³J_{H₅,H₄} = 7.9 Hz, ³J_{H₅,H₆} = 5.8 Hz, 2H, H⁵), 8.45 (d, ³J_{H,H} = 8.0 Hz, 2H, H⁴), 9.23 (d, ³J_{H,H} = 5.8 Hz, 2H, H⁶), 9.53 (s, 2H, H²). ¹³C-NMR (100 MHz, CDCl₃): δ 17.9 (CCH₃), 22.3 (C(CH₃)₂), 31.0 (C(CH₃)₂), 59.2 (CH₃O), 64.7 (CH₂OOC), 69.2, 70.7, 72.0 (CH₂O), 82.4, 88.5 (CH), 102.2, 103.3 (CCH), 126.7 (C⁵), 128.6 (C³), 140.2 (C⁴), 154.4 (C²), 158.4 (C⁶), 163.2 (COO). ³¹P-NMR (162 MHz, CDCl₃): δ -144.2 (sept, J_{P,F} = 713 Hz, PF₆).

3.6. Theoretical Methods

The structures of ligands and complexes were optimized in the Gaussian Program Package [38] based on the previous works [29] without any geometrical constraints. The Global Hybrid Generalized Approximation (GAA) functional B3LYP [39] was used in conjunction with the 6-31+G(d,p) [40] basis set for H, C, O, Cl, and LanL2DZ [41,42] for Ru. Structural and spectroscopic visualizations were performed in the GausView [43] program. The Conductor Like Polarizable Continuum (CPCM) [44] model was employed to optimize structures in chloroform used for the NMR experiments. The NMR spectra were predicted based on the Gauge Independent Atomic Orbital Approach (GIAO) [45,46], as implemented in the Gaussian Program Package. The intramolecular interactions were analyzed using the Natural Bond Orbital Approach (NBO) [47], and their strength was calculated through the second-order perturbation theory.

4. Conclusions

Two neutral ruthenium(II) complexes [RuCl₂(η⁶-*p*-cym)(L-κN)] (L = L2: **2**; L3: **3**) and two cationic complexes [RuCl(η⁶-*p*-cym)(L-κN)₂][PF₆] (L = L1: **4**; L2: **5**) were synthesized. The neutral complexes **1** and **2** were characterized using elemental analysis, ESI-HRMS, IR, and NMR, while the formation of cationic complexes **4** and **5** was investigated using multinuclear NMR spectroscopies. The spectral changes were observed relative to ligand precursors. The Density Functional Theory was applied for the optimization of structures at B3LYP/6-31+G(d,p)(H,C,N,O,Cl)/LanL2DZ(Ru), and structural features were described. The special emphasis was put on the intramolecular interactions, examined using the Natural Bond Orbital Theory and their intensity upon changes in the ligand structure and the number of ligands. The high stability of these compounds was predicted, and further biological studies are advised.

Author Contributions: Conceptualization, D.D. and G.N.K.; methodology, G.N.K. and T.E.; software, D.D. and D.M.; validation, D.M. and T.E.; formal analysis, D.D. and T.E.; investigation, T.E. and D.D.; resources, D.M. and G.N.K.; data curation, D.M.; writing—original draft preparation, T.E. and D.D.; writing—review and editing, D.M. and G.N.K.; visualization, T.E. and D.D.; supervision, G.N.K.; project administration, G.N.K.; funding acquisition, G.N.K. All authors have read and agreed to the published version of the manuscript.

Funding: This research was funded by the Ministry of Science, Technological Development, and Innovation of the Republic of Serbia, contract numbers 451-03-47/2023-01/200146 and 451-03-47/2023-01/200378.

Data Availability Statement: The data presented in this study are available on request from the corresponding author.

Conflicts of Interest: The authors declare no conflict of interest. The funders had no role in the design of the study; in the collection, analyses, or interpretation of data; in the writing of the manuscript; or in the decision to publish the results.

References

1. Arnesano, F.; Natile, G. Mechanistic insight into the cellular uptake and processing of cisplatin 30 years after its approval by FDA. *Coord. Chem. Rev.* **2009**, *253*, 2070–2081. [[CrossRef](#)]
2. Hambley, T.W. Developing new metal-based therapeutics: Challenges and opportunities. *Dalt. Trans.* **2007**, *43*, 4929–4937. [[CrossRef](#)]
3. Monneret, C. Platinum anticancer drugs. From serendipity to rational design. *Ann. Pharm. Françaises* **2011**, *69*, 286–295. [[CrossRef](#)] [[PubMed](#)]
4. Komeda, S.; Casini, A. Next-Generation Anticancer Metallo-drugs. *Curr. Top. Med. Chem.* **2012**, *12*, 219–235. [[CrossRef](#)] [[PubMed](#)]
5. Gómez-Ruiz, S.; Maksimović-Ivanić, D.; Mijatović, S.; Kaluđerović, G.N. On the Discovery, Biological Effects, and Use of Cisplatin and Metallocenes in Anticancer Chemotherapy. *Bioinorg. Chem. Appl.* **2012**, *2012*, 140284. [[CrossRef](#)]
6. Giaccone, G. Clinical Perspectives on Platinum Resistance. *Drugs* **2000**, *59*, 9–17. [[CrossRef](#)] [[PubMed](#)]
7. Thota, S.; Rodrigues, D.A.; Crans, D.C.; Barreiro, E.J. Ru(II) Compounds: Next-Generation Anticancer Metallotherapeutics? *J. Med. Chem.* **2018**, *61*, 5805–5821. [[CrossRef](#)] [[PubMed](#)]
8. Rilak Simović, A.; Masnikosa, R.; Bratsos, I.; Alessio, E. Chemistry and reactivity of ruthenium(II) complexes: DNA/protein binding mode and anticancer activity are related to the complex structure. *Coord. Chem. Rev.* **2019**, *398*, 113011. [[CrossRef](#)]
9. Conti, L.; Macedi, E.; Giorgi, C.; Valtancoli, B.; Fusi, V. Combination of light and Ru(II) polypyridyl complexes: Recent advances in the development of new anticancer drugs. *Coord. Chem. Rev.* **2022**, *469*, 214656. [[CrossRef](#)]
10. Garza-Ortiz, A.; Maheswari, P.U.; Siegler, M.; Spek, A.L.; Reedijk, J. Ruthenium(III) Chloride Complex with a Tridentate Bis(arylimino)pyridine Ligand: Synthesis, Spectra, X-ray Structure, 9-Ethylguanidine Binding Pattern, and In Vitro Cytotoxicity. *Inorg. Chem.* **2008**, *47*, 6964–6973. [[CrossRef](#)]
11. Schuecker, R.; John, R.O.; Jakupec, M.A.; Arion, V.B.; Keppler, B.K. Water-Soluble Mixed-Ligand Ruthenium(II) and Osmium(II) Arene Complexes with High Antiproliferative Activity. *Organometallics* **2008**, *27*, 6587–6595. [[CrossRef](#)]
12. Peacock, A.F.A.; Sadler, P.J. Medicinal Organometallic Chemistry: Designing Metal Arene Complexes as Anticancer Agents. *Chem.—Asian J.* **2008**, *3*, 1890–1899. [[CrossRef](#)] [[PubMed](#)]
13. Renfrew, A.K.; Phillips, A.D.; Egger, A.E.; Hartinger, C.G.; Bosquain, S.S.; Nazarov, A.A.; Keppler, B.K.; Gonsalvi, L.; Peruzzini, M.; Dyson, P.J. Influence of Structural Variation on the Anticancer Activity of RAPTA-Type Complexes: Ptn versus pta. *Organometallics* **2009**, *28*, 1165–1172. [[CrossRef](#)]
14. Therrien, B.; Süß-Fink, G.; Govindaswamy, P.; Renfrew, A.K.; Dyson, P.J. The “Complex-in-a-Complex” Cations [(acac)₂M₂Cu₆(p-*i*PrC₆H₄Me)₆(tpt)₂(dhbq)₃]⁶⁺: A Trojan Horse for Cancer Cells. *Angew. Chem.* **2008**, *120*, 3833–3836. [[CrossRef](#)]
15. Bergamo, A.; Masi, A.; Dyson, P.J.; Sava, G. Bergamo Modulation of the metastatic progression of breast cancer with an organometallic ruthenium compound. *Int. J. Oncol.* **1992**, *33*, 1281–1289. [[CrossRef](#)]
16. Lee, S.Y.; Kim, C.Y.; Nam, T.-G. Ruthenium Complexes as Anticancer Agents: A Brief History and Perspectives. *Drug Des. Devel. Ther.* **2020**, *14*, 5375–5392. [[CrossRef](#)] [[PubMed](#)]
17. Allardyce, C.S.; Dyson, P.J.; Ellis, D.J.; Heath, S.L. [Ru(η^6 -p-cymene)Cl₂(pta)] (pta=1,3,5-triaza-7-phosphatricyclo[3.3.1.1]decane): A water soluble compound that exhibits pH dependent DNA binding providing selectivity for diseased cells. *Chem. Commun.* **2001**, *15*, 1396–1397. [[CrossRef](#)]
18. Therrien, B. Functionalised η^6 -arene ruthenium complexes. *Coord. Chem. Rev.* **2009**, *253*, 493–519. [[CrossRef](#)]
19. Clarke, M.J. Ruthenium metallopharmaceuticals. *Coord. Chem. Rev.* **2002**, *232*, 69–93. [[CrossRef](#)]
20. Smith, G.S.; Therrien, B. Targeted and multifunctional arene ruthenium chemotherapeutics. *Dalt. Trans.* **2011**, *40*, 10793. [[CrossRef](#)]
21. Kenny, R.G.; Marmion, C.J. Toward Multi-Targeted Platinum and Ruthenium Drugs—A New Paradigm in Cancer Drug Treatment Regimens? *Chem. Rev.* **2019**, *119*, 1058–1137. [[CrossRef](#)]
22. Morris, R.E.; Aird, R.E.; del Socorro Murdoch, P.; Chen, H.; Cummings, J.; Hughes, N.D.; Parsons, S.; Parkin, A.; Boyd, G.; Jodrell, D.I.; et al. Inhibition of Cancer Cell Growth by Ruthenium(II) Arene Complexes. *J. Med. Chem.* **2001**, *44*, 3616–3621. [[CrossRef](#)] [[PubMed](#)]
23. Yan, Y.K.; Melchart, M.; Habtemariam, A.; Sadler, P.J. Organometallic chemistry, biology and medicine: Ruthenium arene anticancer complexes. *Chem. Commun.* **2005**, *38*, 4764–4776. [[CrossRef](#)] [[PubMed](#)]
24. Aird, R.E.; Cummings, J.; Ritchie, A.A.; Muir, M.; Morris, R.E.; Chen, H.; Sadler, P.J.; Jodrell, D.I. In Vitro and In Vivo activity and cross resistance profiles of novel ruthenium (II) organometallic arene complexes in human ovarian cancer. *Br. J. Cancer* **2002**, *86*, 1652–1657. [[CrossRef](#)] [[PubMed](#)]
25. Chen, C.; Xu, C.; Li, T.; Lu, S.; Luo, F.; Wang, H. Novel NHC-coordinated ruthenium(II) arene complexes achieve synergistic efficacy as safe and effective anticancer therapeutics. *Eur. J. Med. Chem.* **2020**, *203*, 112605. [[CrossRef](#)] [[PubMed](#)]
26. Muralisankar, M.; Chen, J.-R.; Haribabu, J.; Ke, S.-C. Effective and Selective Ru(II)-Arene Complexes Containing 4,4'-Substituted 2,2' Bipyridine Ligands Targeting Human Urinary Bladder Cancer Cells. *Int. J. Mol. Sci.* **2023**, *24*, 11896. [[CrossRef](#)] [[PubMed](#)]
27. Casini, A.; Karotki, A.; Gabbiani, C.; Rugi, F.; Vašák, M.; Messori, L.; Dyson, P.J. Reactivity of an antimetastatic organometallic ruthenium compound with metallothionein-2: Relevance to the mechanism of action. *Metallomics* **2009**, *1*, 434. [[CrossRef](#)] [[PubMed](#)]
28. Süß-Fink, G.; Khan, F.-A.; Juillerat-Jeanneret, L.; Dyson, P.J.; Renfrew, A.K. Synthesis and Anticancer Activity of Long-Chain Isonicotinic Ester Ligand-Containing Arene Ruthenium Complexes and Nanoparticles. *J. Clust. Sci.* **2010**, *21*, 313–324. [[CrossRef](#)]

29. Eichhorn, T.; Hey-Hawkins, E.; Maksimović-Ivanić, D.; Mojić, M.; Schmidt, J.; Mijatović, S.; Schmidt, H.; Kaluderović, G.N. Binuclear dichlorido(η^6 -p-cymene)ruthenium(II) complexes with bis(nicotinate)- And bis(isonicotinate)-polyethylene glycol ester ligands. *Appl. Organomet. Chem.* **2015**, *29*, 20–25. [[CrossRef](#)]
30. Kaluderović, G.N.; Kommera, H.; Schwieger, S.; Paethanom, A.; Kunze, M.; Schmidt, H.; Paschke, R.; Steinborn, D. Synthesis, characterization, in vitro antitumoral investigations and interaction with plasmid pBR322 DNA of R2eddp-platinum(IV) complexes (R = Et, n-Pr). *Dalt. Trans.* **2009**, *48*, 10720–10726. [[CrossRef](#)]
31. Kaluderović, G.N.; Sabo, T.J. Synthesis and characterization of the cobalt(III) complexes with ethylenediamine-N,N'-di-3-propanoate ligand and its esters. *Polyhedron* **2002**, *21*, 2277–2282. [[CrossRef](#)]
32. Haydock, D.B.; Mulholland, T.P.C. Some derivatives of NN'-biscarboxymethyl- and NN'-bis-(β -carboxyethyl)-ethylenediamine. *J. Chem. Soc. C* **1971**, *13*, 2389–2395. [[CrossRef](#)] [[PubMed](#)]
33. Eichhorn, T.; Kolbe, F.; Mišić, S.; Dimić, D.; Morgan, I.; Saoud, M.; Milenković, D.; Marković, Z.; Ruffer, T.; Dimitrić Marković, J.; et al. Synthesis, Crystallographic Structure, Theoretical Analysis, Molecular Docking Studies, and Biological Activity Evaluation of Binuclear Ru(II)-1-Naphthylhydrazine Complex. *Int. J. Mol. Sci.* **2023**, *24*, 689. [[CrossRef](#)] [[PubMed](#)]
34. Eichhorn, T.; Dimic, D.; Markovic, Z.; Kaludjerovic, G. Synthesis, spectroscopic characterization, and DFT analysis of dichlorido(η^6 -p-cymene)ruthenium(II) complexes with isonicotinate-polyethylene glycol ester ligands. *J. Serbian Chem. Soc.* **2023**, *70*. [[CrossRef](#)]
35. Lalrempuia, R.; Kollipara, M.R.; Carroll, P.J. Syntheses and characterization of arene ruthenium (II) complexes containing N,N'-donor Schiff base ligands. Crystal and molecular structure of $[(\eta^6\text{-C}_6\text{Me}_6)\text{Ru}(\text{C}_5\text{H}_4\text{N-2-CH=N-C}_6\text{H}_4\text{-p-NO}_2)]\text{PF}_6$. *Polyhedron* **2003**, *22*, 605–609. [[CrossRef](#)]
36. Al-Noaimi, M.; AlDamen, M.A. Ruthenium complexes incorporating azoimine and α -diamine based ligands: Synthesis, crystal structure, electrochemistry and DFT calculation. *Inorganica Chim. Acta* **2012**, *387*, 45–51. [[CrossRef](#)]
37. Savić, A.; Dulović, M.; Poljarević, J.M.; Misirlić-Denčić, S.; Jovanović, M.; Bogdanović, A.; Trajković, V.; Sabo, T.J.; Grgurić-Šipka, S.; Marković, I. Synthesis and in vitro Anticancer Activity of Ruthenium–Cymene Complexes with Cyclohexyl-Functionalized Ethylenediamine-N,N'-diacetate-Type Ligands. *ChemMedChem* **2011**, *6*, 1884–1891. [[CrossRef](#)]
38. Frisch, M.J.; Trucks, G.W.; Schlegel, H.B.; Scuseria, G.E.; Robb, M.A.; Cheeseman, J.R.; Scalmani, G.; Barone, V.; Mennucci, B.; Petersson, G.A.; et al. *Gaussian 09, Revision C.01*; Gaussian, Inc.: Wallingford, CT, USA, 2009.
39. Becke, A.D. Density-functional thermochemistry. III. The role of exact exchange. *J. Chem. Phys.* **1993**, *98*, 5648. [[CrossRef](#)]
40. Dunning, T.H. Gaussian basis sets for use in correlated molecular calculations. I. The atoms boron through neon and hydrogen. *J. Chem. Phys.* **1989**, *90*, 1007. [[CrossRef](#)]
41. Hay, P.J.; Wadt, W.R. Ab initio effective core potentials for molecular calculations. Potentials for the transition metal atoms Sc to Hg. *J. Chem. Phys.* **1985**, *82*, 270–283. [[CrossRef](#)]
42. Hay, P.J.; Wadt, W.R. Ab initio effective core potentials for molecular calculations. Potentials for K to Au including the outermost core orbitals. *J. Chem. Phys.* **1985**, *82*, 299–310. [[CrossRef](#)]
43. Dennington, R.; Todd, K.; Millam, J. *GausView 2009*; Semichem Inc.: Shawnee Mission, KS, USA, 2016.
44. Marenich, A.V.; Cramer, C.J.; Truhlar, D.G. Universal solvation model based on solute electron density and on a continuum model of the solvent defined by the bulk dielectric constant and atomic surface tensions. *J. Phys. Chem. B* **2009**, *113*, 6378–6396. [[CrossRef](#)] [[PubMed](#)]
45. Wolinski, K.; Hinton, J.F.; Pulay, P. Efficient implementation of the gauge-independent atomic orbital method for NMR chemical shift calculations. *J. Am. Chem. Soc.* **1990**, *112*, 8251–8260. [[CrossRef](#)]
46. Ditchfield, R. Self-consistent perturbation theory of diamagnetism. *Mol. Phys.* **1974**, *27*, 789–807. [[CrossRef](#)]
47. Reed, A.E.; Weinstock, R.B.; Weinhold, F. Natural population analysis. *J. Chem. Phys.* **1985**, *83*, 735–746. [[CrossRef](#)]

Disclaimer/Publisher's Note: The statements, opinions and data contained in all publications are solely those of the individual author(s) and contributor(s) and not of MDPI and/or the editor(s). MDPI and/or the editor(s) disclaim responsibility for any injury to people or property resulting from any ideas, methods, instructions or products referred to in the content.